Acta Biomaterialia 71 (2018) 86–95

Contents lists available at ScienceDirect

Acta Biomaterialia

journal homepage: www.elsevier.com/locate/actabiomat

Full length article

Exogenous mineralization of hard tissues using photo-absorptive minerals and femto-second lasers; the case of dental enamel

A.D. Anastasiou [a,*], S. Strafford [b], C.L. Thomson [c], J. Gardy [a], T.J. Edwards [c], M. Malinowski [b], S.A. Hussain [c,d], N.K. Metzger [c], A. Hassanpour [a], C.T.A. Brown [c], A.P. Brown [a], M.S. Duggal [b,e], A. Jha [a]

[a] School of Chemical and Process Engineering, University of Leeds, Leeds LS2 9JT, UK
[b] Leeds Dental School, Worsley Building, University of Leeds, Leeds LS2 9JT, UK
[c] SUPA, School of Physics and Astronomy, University of St Andrews, North Haugh, St Andrews, Fife KY16 9SS, UK
[d] Cambridge Graphene Centre, Engineering Department, University of Cambridge, 9, JJ Thomson Avenue, Cambridge CB3 0FA, UK
[e] School of Dentistry, The National University of Singapore, Singapore

ARTICLE INFO

Article history:
Received 21 November 2017
Received in revised form 5 February 2018
Accepted 9 February 2018
Available online 17 February 2018

Keywords:
Enamel
Laser sintering
Photothermal
Fluorapatite
Iron oxide nanoparticles

ABSTRACT

A radical new methodology for the exogenous mineralization of hard tissues is demonstrated in the context of laser-biomaterials interaction. The proposed approach is based on the use of femtosecond pulsed lasers (fs) and Fe^{3+}-doped calcium phosphate minerals (specifically in this work fluorapatite powder containing Fe_2O_3 nanoparticles (NP)). A layer of the synthetic powder is applied to the surface of eroded bovine enamel and is irradiated with a fs laser (1040 nm wavelength, 1 GHz repetition rate, 150 fs pulse duration and 0.4 W average power). The Fe_2O_3 NPs absorb the light and may act as thermal antennae, dissipating energy to the vicinal mineral phase. Such a photothermal process triggers the sintering and densification of the surrounding calcium phosphate crystals thereby forming a new, dense layer of typically ~20 μm in thickness, which is bonded to the underlying surface of the natural enamel. The dispersed iron oxide NPs, ensure the localization of temperature excursion, minimizing collateral thermal damage to the surrounding natural tissue during laser irradiation. Simulated brushing trials (pH cycle and mechanical force) on the synthetic layer show that the sintered material is more acid resistant than the natural mineral of enamel. Furthermore, nano-indentation confirms that the hardness and Young's modulus of the new layers are significantly more closely matched to enamel than current restorative materials used in clinical dentistry. Although the results presented herein are exemplified in the context of bovine enamel restoration, the methodology may be more widely applicable to human enamel and other hard-tissue regenerative engineering.

Statement of significance

In this work we provide a new methodology for the mineralisation of dental hard tissues using femtosecond lasers and iron doped biomaterials. In particular, we demonstrate selective laser sintering of an iron doped fluorapatite on the surface of eroded enamel under low average power and mid-IR wavelength and the formation of a new layer to substitute the removed material. The new layer is evaluated through simulated brushing trials and nano-indentation. From the results we can conclude that is more acid resistant than natural enamel while, its mechanical properties are superior to that of current restorative materials. To the best of our knowledge this is the first time that someone demonstrated, laser sintering and bonding of calcium phosphate biomaterials on hard tissues. Although we here we discuss the case of dental enamel, similar approach can be adopted for other hard tissues, leading to new strategies for the fixation of bone/tooth defects.

1. Introduction

Mineralized tissues are composite structures consisting of an inorganic mineral phase (hydroxyapatite), organic material, and

* Corresponding author.
E-mail address: a.anastasiou@leeds.ac.uk (A.D. Anastasiou).

https://doi.org/10.1016/j.actbio.2018.02.012
1742-7061/

cells [1]. A very special case of hard tissue is dental enamel which presents a unique microstructure and extraordinary mechanical properties as it is the hardest tissue of the human body. Although initial mineralisation of enamel occurs in a protein rich environment, the inorganic content in mature enamel decreases to <5% wt [2] this process makes enamel an acellular and avascular tissue that lacks an intrinsic regenerative capacity, in contrast to bone and dentine.

In everyday life, teeth are exposed to various physical and chemical oral challenges including mastication, abrasion and acid erosion. Acid erosion and wear are common occurrences in human enamel which progressively weaken teeth, and these can readily progress to expose both dentine and the micro-channels (dentine tubules) below the enamel layer, of teeth. Oral fluid ingress of the micro-tubules during eating and drinking can then trigger the mechanoreceptor nerves at the root of the dentine structure to cause pain. This condition is known as dentine hypersensitivity (DH) [3]. At present there is no long lasting treatment available for acid erosion since, most of the available clinical and personal care treatments offer only temporary symptomatic control (e.g. branded toothpastes and fluoride treatment). A more invasive strategy is to coat the tooth with photo-active acrylic or composite materials to occlude the dentine tubules however, these materials are structurally incompatible with enamel due to differences in thermal expansion coefficients and Young's moduli [3]. These mechanical differences can lead to the failure of the coating in the longer term [4].

This lack of a permanent solution led to the development of biomimetic restorative approaches which imitate the natural physiological functions of dentine and enamel tissue. The most promising among these techniques is the use of self-assembling peptide scaffolds. For example, rationally designed β-sheet-forming peptides can spontaneously assemble to form 3D biomimetic scaffolds capable of nucleating hydroxyapatite de novo in response to environmental triggers [5]. During preclinical studies the use of an anionic peptide (P_{11}-4) proved capable of in situ enamel regeneration however, took more than 30 days of treatment to enable a significant change of size of a pre-existing dental lesion [6]. Another biomimetic approach involves the formation of new hydroxyapatite crystals on etched enamel coated with poly amido amine (PAMAM) dendrimers [7]. PAMAM-COOH can act as the organic template on an enamel surface that trigger the formation of hydroxyapatite crystals of the same orientation as the natural tissue. Although many of these techniques have demonstrated some potential, they are still far from clinical translation and application in theatre. A successful treatment should be easy-to-apply by clinicians and more importantly should have the potential for rapid enamel restoration indigenously or exogenously.

It is apparent that there is a clear need for a better solution to enamel restoration, which supersedes the performance of current treatments. In this respect, we have already identified an exogenous remineralisation procedure for enamel that combines the intensity of a femtosecond (fs) pulsed near-IR laser (e.g. 1520 nm or 1045 nm) with photo-active rare-earth (RE^{3+}) or Fe^{3+}-doped calcium phosphate minerals [8,9]. In this approach a fresh calcium phosphate biomaterial is pasted on to a defective area of a tooth, to produce a thin, loosely adherent film (<30 μm). A fs pulsed laser is then used to selectively sinter, densify and bond the new material to the underlying tooth surface. A pivotal factor for the successful outcome of the proposed methodology and for its future translation to the clinic, is to control and minimise any thermal effects induced by the laser. According to Niemz [10], the extent and degree of tissue damage during interaction with a laser beam, depends both on the irradiation parameters of the laser (e.g. wavelength, average energy, pulse duration and exposure time) and the optical properties of the tissue (e.g. absorption and scattering coefficients at the irradiation wavelength). Here, we demonstrated that femtosecond laser pulses and photoactive doping of calcium phosphate materials limits heat build-up and minimises the risk of any thermally induced necrosis in the surrounding healthy tissue; e.g. on gums and underlying dentine.

In clinical dentistry, high-power (~5 W) continuous wave CO_2 lasers (operating at 9.6–10.6 μm wavelength) and Q-switched RE^{3+}-doped crystal lasers (at 1.064 μm wavelength in Nd^{3+}- and 2.940 μm wavelength in Er^{3+}-doped YAG) are already used to induce permanent alterations of irradiated enamel surfaces (e.g. laser-induced melting). Such procedures accumulate heat increasing the risk of collateral damage of the underlying dentine and the surrounding sensitive soft tissues (e.g. nerves and gums). For acid-eroded enamel restoration however, tissue needs rebuilding (and not melting), rendering the above irradiation conditions inappropriate. In the present work experiments have been conducted with a high repetition fs pulsed laser, emitting at 1045 nm wavelength which was found suitable for confining thermal effects only to the irradiated area [9]. Pulsed near infrared laser irradiation (between 700 nm and 2500 nm wavelength), enables higher spatial accuracy and sintering at lower average powers (<5 W) than a continuous wave laser [11].

The goal in this work is to demonstrate the formation of a dense, well bonded mineral layer on bovine tooth enamel with minimal alteration of the underlying structure. For the experiments, synthetic fluorapatite (FAP) particles are applied to enamel surfaces; the presence of fluoride ions is desirable to inhibit enamel demineralisation and prevent bacterial colonization of gums, which are the underpinning cause of periodontitis [12]. The incorporation of Fe^{3+}-ions in fluorapatite increases the linear absorption of the ultra-short pulsed near-IR photons at 1045 nm wavelength further enhancing localised mineral densification [9]. After irradiation experiments the new layers are characterised by X-ray diffraction, SEM and EDX to identify the resulting phase transformations, and to evaluate the post-sintering morphology of the new surface. Surface hardness and Young's modulus are measured by nano-indentation while, simulated brushing trials are conducted to test how the abrasion resistance of the new surface compares to that of the natural enamel.

2. Materials and methods

2.1. Materials synthesis and sample preparation

The synthesis of the Fe containing fluorapatite followed the precipitation method described elsewhere [13]. Specifically, 200 ml of a 0.1 M $Ca(NO_3)_2$ $4H_2O$ (Fisher Chemicals, CAS:13477-34-4) aqueous solution, containing 0.8 g $Fe(NO_3)_3{\cdot}9H_2O$ (Sigma Aldrich, CAS:7782-61-8) was prepared (solution A) and then heated to 50 °C. At temperature, 1 M $(NH_4)_3PO_4$ (Acros Organics, CAS:7783-28-0) solution (200 ml) containing the appropriate mass of NH_4F for stoichiometric fluorapatite, was introduced dropwise into the solution (A). To maintain pH above 9, a 0.1 M NaOH solution was also added during mixing. The addition of NaOH results in the deprotonation of the Fe^{2+} and Fe^{3+} ions and the formation of Fe $(OH)_y^{2-y}$ structures. The final mixture was continuously stirred at 50 °C for 2 h and then left to settle for 1 h to allow precipitation. In these conditions we also have the dehydration of the $Fe(OH)_y^{2-y}$ and the precipitation of hematite nanoparticles [14]. The agglomerated Fluorapatite crystals and the hematite nanoparticles (which are trapped within the FAP agglomerates) were collected on a filter paper (Whatman grade 44 with pores of 1 μm), washed several times with distilled water and then dried for 24 h at 80 °C. After drying the powder was heat treated to 400 °C for 3 h.

Bovine enamel blocks were prepared by cutting square pieces approximately 2 mm wide with Well Diamond Wire Saw, water-cooled, cutting machine (Well® Walter EBNER, CH-2400 Le Loche). The blocks were mounted in epoxy resin (Stycast 1266) before grinding the enamel surface flat using wet/dry paper. An artificial lesion with dimensions 2 x 1 x 0.02 mm (L × W × D) was created on each sample by exposing the area in the center of the block to a citric acid solution (pH 3.7) for one day. The topology of each block was then characterized using non-contact profilometry (ProScan 2000, Scantron Industrial Products Limited, Somerset, England).

To powder coat each sample, 0.3 g of FAP was dispersed in 20 ml of an aqueous acetic acid solution (1% v/v). 0.1 g of high molecular weight chitosan powder (Sigma Aldrich 419419) was added to the solution and left to dissolve under continuous stirring. 50 µml of the chitosan/mineral mixture was applied to the surface of each dental sample using a single channel pipette, making sure that the lesion was completely covered and then left to dry for 10 min at room temperature. As the coating dries and the volume of the liquid phase is reduced, the suspended crystals are drawn together, the chitosan forms an adherent film on the enamel and a relatively dense layer of FAP becomes fixed to the surface of the lesion.

The fs-laser irradiation experiments were performed with an ultrafast, pulsed source from a single crystal cavity of Yb:KGW (developed in-house at St Andrews University). Typical pulse duration of the laser were adjusted to be between 130 and 190 fs with an emission wavelength at 1045 nm and a repetition rate of 1 GHz. The coated enamel blocks were placed on a 3-axis motorised translation stage, controlled by a LabView routine in order to have a zig-zag irradiation pattern (with 30 µm spacing between the lines). The total irradiated area was a rectangular section with dimensions 1 × 2 mm, and was large enough to expose the entire coated artificial lesion. During the laser irradiation experiments the average laser power was adjusted to 0.40 W (measured at the output of the source), the scanning velocity was 50 µm/s and the spot diameter was 30 µm. The average intensity was 14 kW/cm^2 with a peak power intensity of 95 MW/cm^2 (150 fs pulse duration.) Each spot of the coating was irradiated for a total of 0.6 s giving an accumulated energy of 0.24 J per spot.

2.2. Characterisation techniques

The phase constitution of crystalline material formed during synthesis was analysed by a Philips X'Pert MPD X-Ray powder diffractometer equipped with a monochromatic Cu Kα radiation source (0.154098 nm). A step size of 0.065° and a 2θ scanning range from 10° to 60°, was used at a scan speed of 0.014132°s^{-1} to yield a powder diffraction pattern.

A Hitachi SU8230 Scanning electron microscopy (SEM), operating at 10 keV and fitted with a cold field emission gun and Oxford Instruments 150 mm^2 SD energy dispersive X-ray (EDX) detector was used for morphological and phase composition analysis of the sintered layers of minerals. Prior to SEM analysis, it was necessary to coat the calcium phosphate mineral surface with a 5 nm thin layer of platinum followed by vacuum cleaning for 10 min (Quorum Technologies sputter coater and vacuum cleaner) to minimize electrostatic charging during analysis.

For TEM imaging, powder samples were dispersed in ethanol and a drop of the suspension was placed onto a Lacey Carbon Film (Agar Scientific Ltd). Imaging and analysis of the samples was performed with a FEI Titan-cubed, Themis 300 Transmission Electron Microscope (TEM) equipped with multiple HAADF/ADF/BF STEM detectors and a FEI Super-X, 4-detector EDX system.

The mechanical properties of the sintered layers were measured using a NanoTest machine, equipped with a Berkovic intender and manufactured by Micro Materials Ltd., Wrexham, UK. For each sample, several points were tested with three different loads (i.e. 50, 100 and 150 mN) and an average value was obtained. Experimental values for hardness (H, GPa) and Young Modulus (GPa) acquired by processing the experimental data with the NanoTest software.

3. Results

3.1. X-ray diffraction

The diffraction pattern of the synthesised mineral, after heat treatment and before laser irradiation, shows by comparison to reference XRD data on fluorapatite (01-087-2462) that the only detectable phase is FAP (Fig. 1a). Diffraction peak analysis does however show that a systematic shift in the peaks of between 0.05 and 0.2° to larger 2θ values (Fig. 1b). This shift indicates that a fraction of the ferrous ions are incorporated into the FAP lattice. Substitution of Ca^{2+}(0.99 Å) with Fe^{2+}(0.74 Å) /Fe^{3+}(0.64 Å) ions, which are significantly smaller than Ca^{2+}-ions, result in a proportionate shrinkage in the unit cell volume of apatite. XRD of the

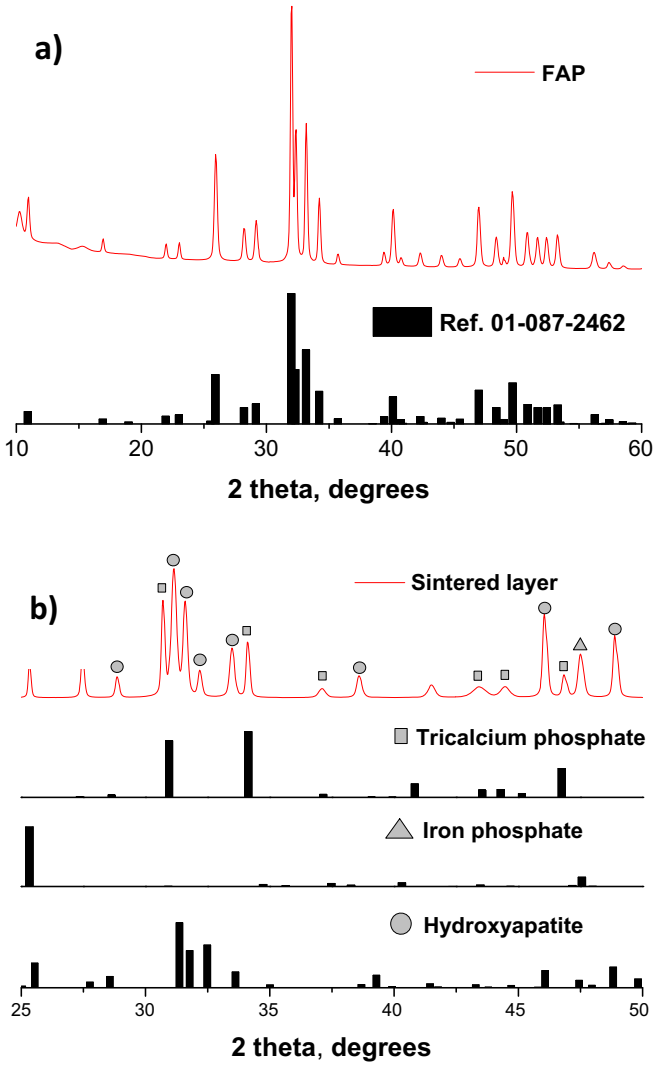

Fig. 1. X-Ray diffraction patterns of a) the as-synthesized fluorapatite powder (after heat treatment); b) laser-sintered Fe-containing fluorapatite coating on enamel surface. Reference patterns of phases identified in the experimental patterns are shown below.

laser-sintered material on enamel shows that there are significant changes in phase, compared with the starting mineral (Fig. 1b). The dominant phase in the sintered material is tricalcium phosphate (TCP) with intense diffraction peaks at 2θ° = 30.71, 34.09, 43.4, 44.4 and 46.8. The presence of TCP has been reported in many other works involving thermal sintering of hydroxyapatite and FAP powders, typically forming over a temperature range of 1000–1400 °C [15,16]. The peaks at 2θ = 25.32° and 47.50° can be assigned to a newly formed iron phosphate phase ($FePO_4$). Finally, there are many peaks (i.e. 2θ° = 31.12, 31.57, 32.20, 33.50, 38.65, 46.05, 48.90) matching the diffraction pattern of HAP and may be attributed to the mineral of enamel. Since, the thickness of the coating is almost 20 μm and given that the penetration depth of Cu Ka X-rays can be between 20 and 120 μm (depending on the incident angle), some of the peaks are expected to derive from the hydroxyapatite of the underlying enamel.

3.2. Transmission electron microscopy (TEM)

TEM identified the presence of clusters of iron oxide nanoparticles (NPs) mixed with the FAP nanocrystals in the synthesized mineral powder (Fig. 2). Elemental X-ray maps produced by SEM-EDX show a homogeneous distribution of O (Fig. 2b), Ca (Fig. 2c) and P (Fig. 2e) across the entire area analysed by TEM, the iron-rich phase is however localised, (Fig. 2d). Selected area electron diffraction patterns (SAEDP) of the iron-rich regions revealed d-spacings that correspond to those for hematite (Fe_2O_3) (ref. 01-089-0597 specifically for reflexions from planes (0 1 2), (1 0 4), (1 1 0), (0 2 4) and (1 1 6)). Iron oxide nanoparticles can be synthesised by co-precipitation of Fe^{2+} or Fe^{3+} from solution at low pH by the addition of a base [14]. These conditions are satisfied during the FAP synthesis route, since the Fe is added in solution (from $Fe(NO_3)_3 \cdot 9H_2O$) and the pH is maintained above 9 by the addition of NaOH. Consequently, the presence of hematite is justified while a fraction of the initial Fe^{3+} is expected to have been incorporated into the mineral's lattice (as is supported by the X-ray diffraction patterns above).

3.3. Scanning electron microscopy (SEM)

Typical images of the pre- and post-sintered coating on the enamel surface show a clear change in morphology of the pre and post irradiated coating (Fig. 3). The applied coating is relatively flat and homogeneous, in which individual aggregated crystals of FAP may be seen in spheruletic morphologies (Fig. 3b). After laser irradiation the new layer covering the whole area of the artificial lesion appears homogenous, compact and densified (Fig. 3c and 3d; the tracks of each laser pass may be seen at both low and high-magnification for comparison). There is however some evidence for micro-cracking, likely resulting from thermal stress developed during sintering. The SEM EDX elemental mapping enables us to identify the interface between the uncoated enamel and the new layer, since in the latter the concentration of iron oxide is much higher (Fig. 3e and f). The EDX maps show how the chemical composition of the sintered layer is inhomogeneous (Fig. 3 g, h, i and j). The dominant phase is sintered tricalcium phosphate (TCP) as identified by XRD (Fig. 1) with discretely distributed lamellae where the concentration of iron is elevated (Fig. 3i). The presence of an iron-rich phase is consistent with the presence of $FePO_4$ in the XRD of the sintered layer (Fig. 1b).

3.4. Evaluation of thermal induced damage to enamel

Cross-sections of the sintered samples were imaged by SEM in order to evaluate any alterations induced into the coated enamel by heat diffusion during the laser irradiation. Both the sintered layer and the underlying enamel are compact and there is no significant cracking due to thermal stresses or any other sign of thermal damage (Fig. 4a) although, high magnification imaging of the sintered layer/enamel interface, reveals the presence of some nano-porosity in the enamel and within a distance of only 1–2 μm below the sintered layer (Fig. 4b).

We have shown previously that it is possible to estimate the scale and temperature of the heat affected zone around a laser irradiated area by measuring the oxygen concentration within the surrounding mineral phase [9]. The same approach has been adopted here for ascertaining potential thermal damage on dental enamel due to laser heating. To establish the heat profile on enamel, data from scanning thermal analysis (STA) were first taken to show that the enamel loses 3.5% of its initial mass upon heating to 1000 °C (Fig. 4d). The mass loss is due to the evolution of CO_2 and water vapor [17]. The loss of CO_2 and H_2O changes the overall oxygen (O) content of the enamel significantly and this can be used as a marker for the characterization of thermal damage induced by laser irradiation. Changes in oxygen concentration with increasing distance from an irradiated area (as measured by SEM-EDX) are compared to the oxygen content of non-irradiated samples of enamel (containing 47 wt% O) and enamel heated at 400, 600 and 900 °C. The material in direct contact with the sintered layer has the highest amount of oxygen (i.e. 57 wt%) and this is significantly higher than that of healthy enamel (Fig. 4e). Moreover, in the same area traces of Fe were identified as well the expected Ca, P and O (Fig. 4c), which implies that during sintering, there might have been diffusion or mass transfer across the materials interface leading to an increased amount of oxygen in the matrix. The lowest oxygen concentration was measured to be 42 wt% at 5 μm below the interface. This is a clear indication of compositional alteration of the underlying enamel due to heat diffusion and this oxygen concentration corresponds to a thermal treatment temperature of around 900 °C. These chemical changes are however restricted to a very narrow zone, since the oxygen content returns to normal levels (i.e. 49 wt%) at a distance of 10 μm from the interface and remains around this value for the rest of the tested points (Fig. 4e).

3.5. Brushing trials and mechanical testing

The results of the 15-day long simulated tooth brushing trials provide a comparison between a sintered layer and natural uncoated enamel (Fig. 5). As reported before [18], the depth of erosion for natural enamel increases linearly over the brushing period, resulting in erosion up to 12 μm deep by the end of a 15-day long cycle. In comparison, the sintered FAP layer is almost wear-resistant with little or no apparent demineralization and minimal mass loss. During the first five days of testing, the sintered material lost a layer only of 1 to 2 μm thick and after this there was no further significant mass-loss over 15 days. Generally, the naturally formed hydroxyapatite mineral in enamel is easily carbonated via anionic substitutions in the mineral crystal lattice, as a result it becomes more acid soluble than other minerals e.g. pure hydroxyapatite, fluorapatite or tricalcium phosphate [19]. This high solubility in combination with the abrasive mechanical forces applied during brushing, makes enamel more vulnerable to demineralization and mass loss and in contrast explains the better performance of the acid resistant FAP-TCP sintered layer.

Typical load-displacement curves for nano-indentation tests are shown in Fig. 6a. The hardness is then calculated from following equation:

$$H = \frac{P_{max}}{A} \quad (1)$$

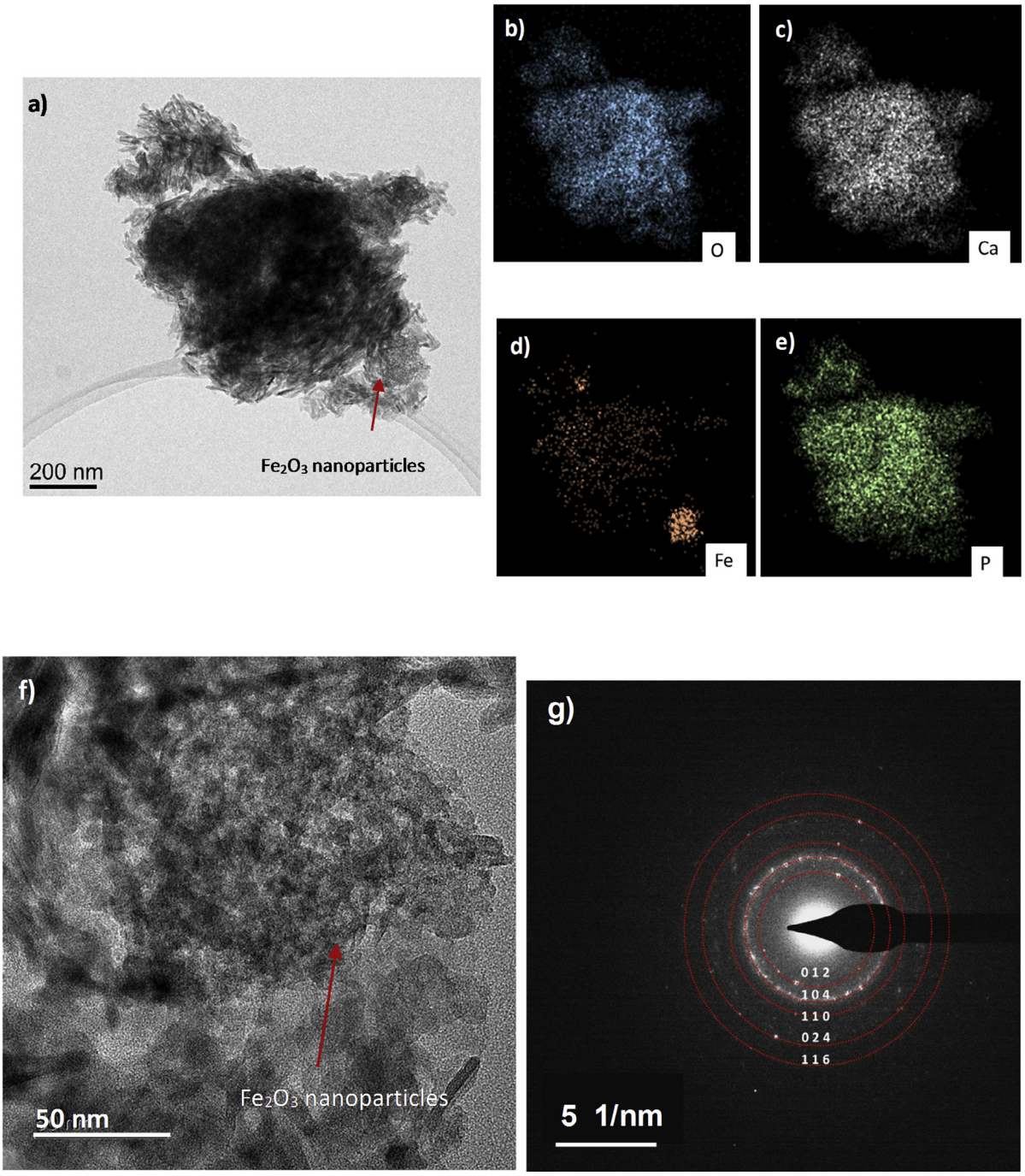

Fig. 2. TEM images of; a) an agglomerate of FAP particles that have the characteristic acicular morphology of an apatite phase (the arrow indicates a cluster of Fe oxide NPs); b) EDX elemental maps for oxygen ($K\alpha$); c) calcium ($K\alpha$); d) iron ($K\alpha$); and e) phosphorus ($K\alpha$); showing the inhomogeneous distribution of iron f) higher magnification bright field TEM image Identification of the iron oxide nanoparticles which are more spherical and clustered together than the acicular FAP particles; g) Selected Area Diffraction patterns (SAED) of the iron rich region showing it to be polycrystalline and with d spacing values that match the reference pattern of hematite (Fe_2O_3).

Where, P_{max} is defined as the maximum applied load (mN), A is the projected indentation area (nm^2) and H is the hardness (mN/nm^2, but converted to GPa). The projected area is determined by the depth of impression (h_c) and the known angle of the indenter as shown in Eq. (2):

$$A = 3\sqrt{3}h_c^2 \tan^2(65) \quad (2)$$

After nano-indentation, the mean hardness of the sintered layer is found to be 1.1 ± 0.16 GPa which is lower than the value for natural enamel at 3.1 ± 0.12 GPa (Fig. 6 and Table 1). Clearly, the new layer is not mechanically superior to enamel however it is significantly harder than the current restorative materials like microhybrid resins (~0.70 GPa) and nanofilled resins (~0.66 GPa) [20]. Also it is harder than other natural human hard tissues which reveals the potential for more tissue engineering applications of this technology (hardness of human femur is around 0.58 GPa) [21]. The deviation of the hardness at different points of the sample from the mean value is quite high for the sintered layer (15% error bars in Fig. 6a). It is well known that the initial density of the coating affects the densification and the mechanical properties of the product of sintering, thus these discrepancies are attributed to

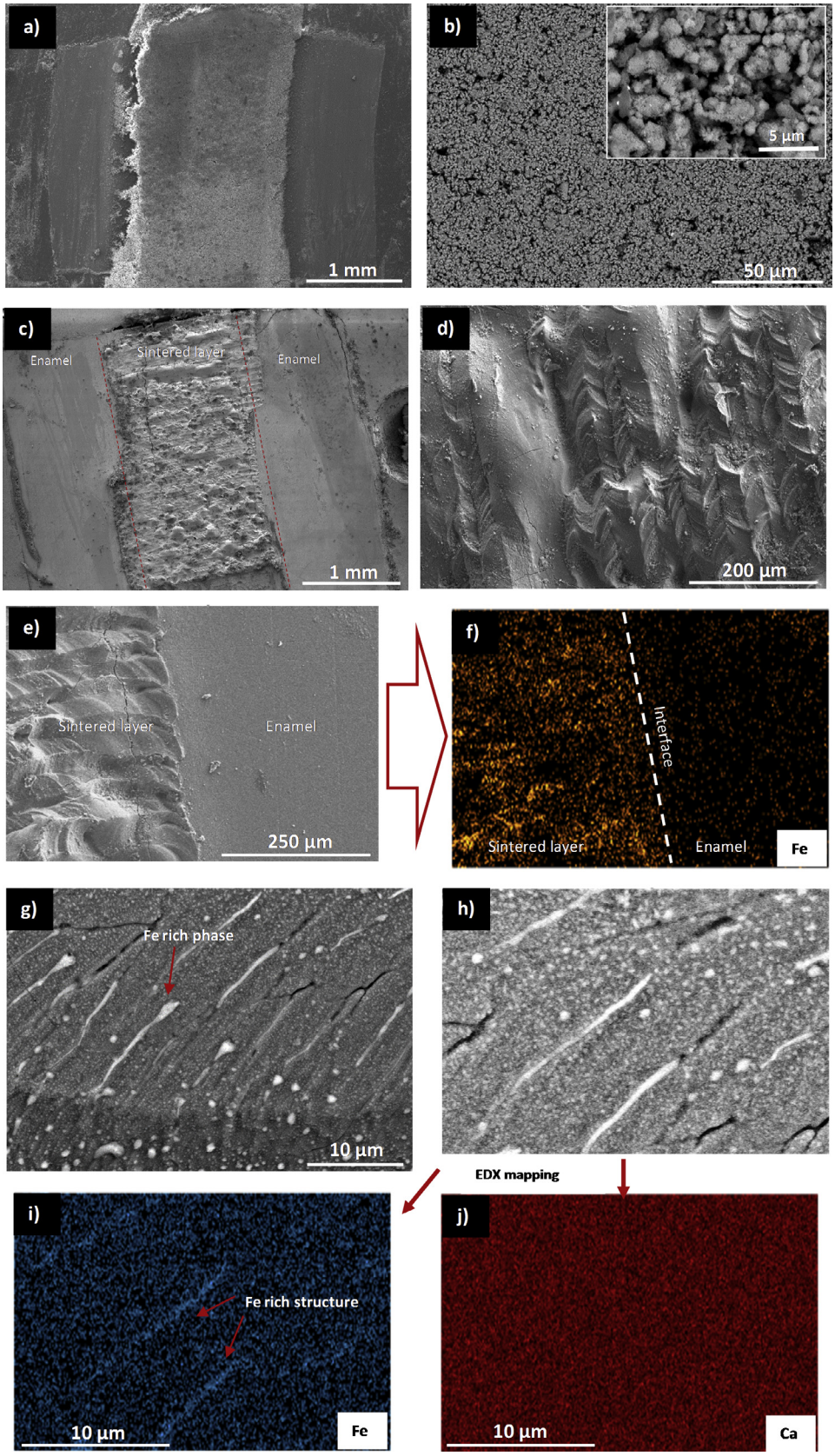

Fig. 3. Scanning Electron Microscopy (SEM) images of a typical pre and post sintered FAP coating on bovine enamel blocks; a) as-deposited FAP coating on dental enamel before laser irradiation; b) high magnification of the FAP aggregates before laser irradiation; c) laser sintered FAP layer on dental enamel; d) higher magnification of the dense, sintered layer also indicating the marks left by the vertical laser tracks; e) identification of the interface between the sintered layer and the enamel; f) EDX mapping of Fe ($K\alpha$) at the interface; g) high magnification back scattered electron image of the sintered layer (top), enamel (bottom) and identification of bright, iron rich lamellar within the sintered layer; h) backscattered electron image of an EDX mapping area of the sintered layer; i) Fe ($K\alpha$) EDX map showing the concentration of Fe in the lamellar; j) Ca ($K\alpha$) EDX map showing a homogeneous distribution of Ca.

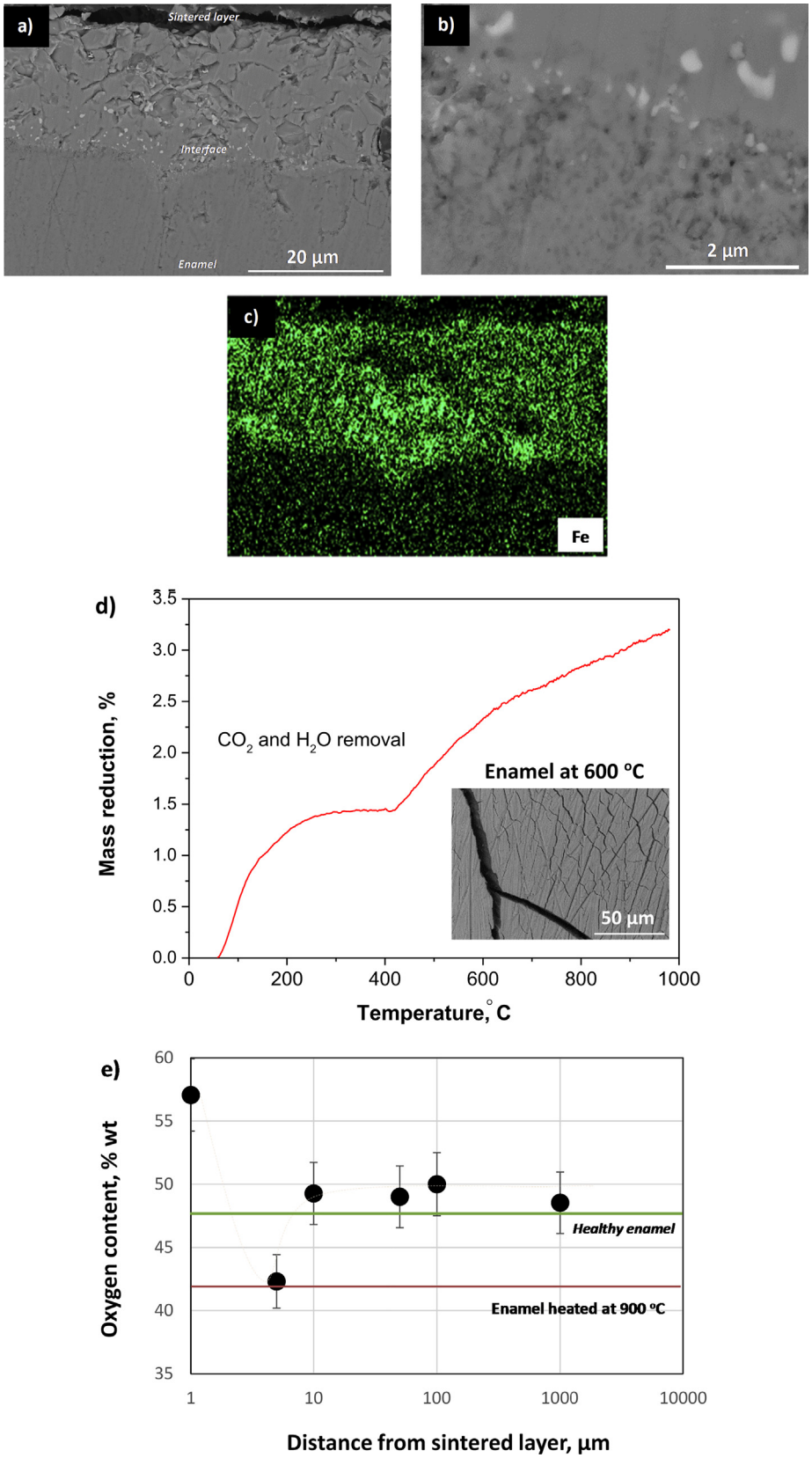

Fig. 4. Evaluation of the thermal effects of laser irradiation on the underlying enamel; a) Cross section of the sintered layer and the underlying enamel; b) High magnification image of the interface between the sintered layer and the enamel reveals some porosity at the surface of the enamel; c) EDX elemental mapping of Fe to identify the sintered layer/enamel interface; d) TGA of enamel for temperatures between 30 and 1000 °C at a heating rate of 20 °C/min, the mass loss is attributed to water and CO_2 loss from the enamel; e) Estimated oxygen content as a function of the distance from the sintered layer/enamel interface suggesting that the enamel is only altered within 10 µm of the interface.

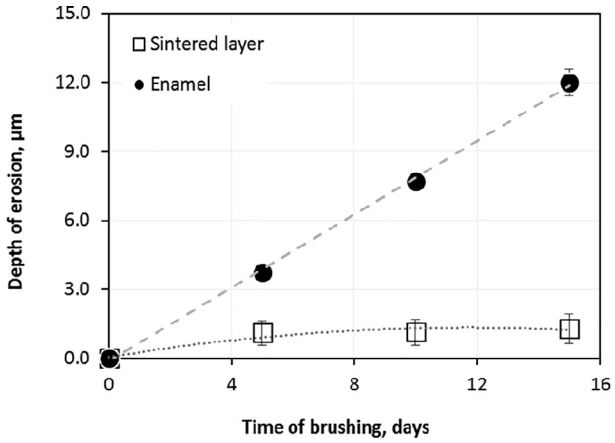

Fig. 5. Erosion depth over 15 days of simulated tooth brushing trials; a comparison between uncoated bovine enamel and the sintered layer of FAP on bovine enamel blocks shows the new layer to be by far superior (5% error bars).

the non-uniform morphology and density of the initial coating. Hysteresis load – displacement data of the sintered layer and the enamel indented with a load of 50 mN show that the indenter displacement at the peak load (h_{max}) is about 1580 nm for the sintered layer and about 1130 nm for enamel which is reasonable since enamel hardness is higher (Fig. 6b).

Reduced modulus (E_r) is the modulus that incorporate the combined moduli of the specimen (E_s) and the indenter (E_i) to account for the deformation of the probe. It can be calculated from the stiffness (S), the slope of the unloading curve of the indentation plot, and the plastic area (A) using following equation, [22]:

$$E_r = \frac{\sqrt{\pi}}{2}\frac{S}{\sqrt{A}} \tag{3}$$

The elastic modulus of the tested materials was calculated based on the equation proposed by Olivier and Pharr, [22].

$$\frac{1}{E_r} = \frac{(1-\upsilon_s^2)}{E_s} + \frac{(1-\upsilon_i^2)}{E_i} \tag{4}$$

Here, E_r is the reduced modulus (for each measurement), v_s is the Poisson's ratio for the sample, v_i is the Poisson's ratio for the intender (0.07 for our system), E_s is the Young's modulus for the system and E_i is the Young's modulus for the intender (1141 GPa for our system). For enamel and the sintered FAP, Poisson's ratios were taken to be 0.25 and 0.27 respectively [23,24]. From Eq. (4), the Young's modulus for the enamel is calculated to be 38 ± 1.9 GPa and for the sintered layer 20.5 ± 1.2 GPa. As in the case of the hardness measurements, the derived value of elastic modulus for the sintered layer is lower than that for natural enamel (Table 1). However, if we compare the values with the current restorative materials and with other human hard tissues the overall mechanical properties of the sintered layer are a significantly better match to enamel ensuring better brushing wear resistance.

4. Discussion

The presence of the iron oxide nanoparticles (NPs) in the starting FAP mineral enhances laser sintering in the ultrafast regime, which is beneficial given that the average laser power used here is much lower than that used in clinical dentistry for tissue ablation. In general, metal oxide NPs generate heat when they are irradiated with a laser. This property is known as the photothermal effect and has been studied intensively for various biomedical applications e.g. simultaneous molecular imaging and for cancer

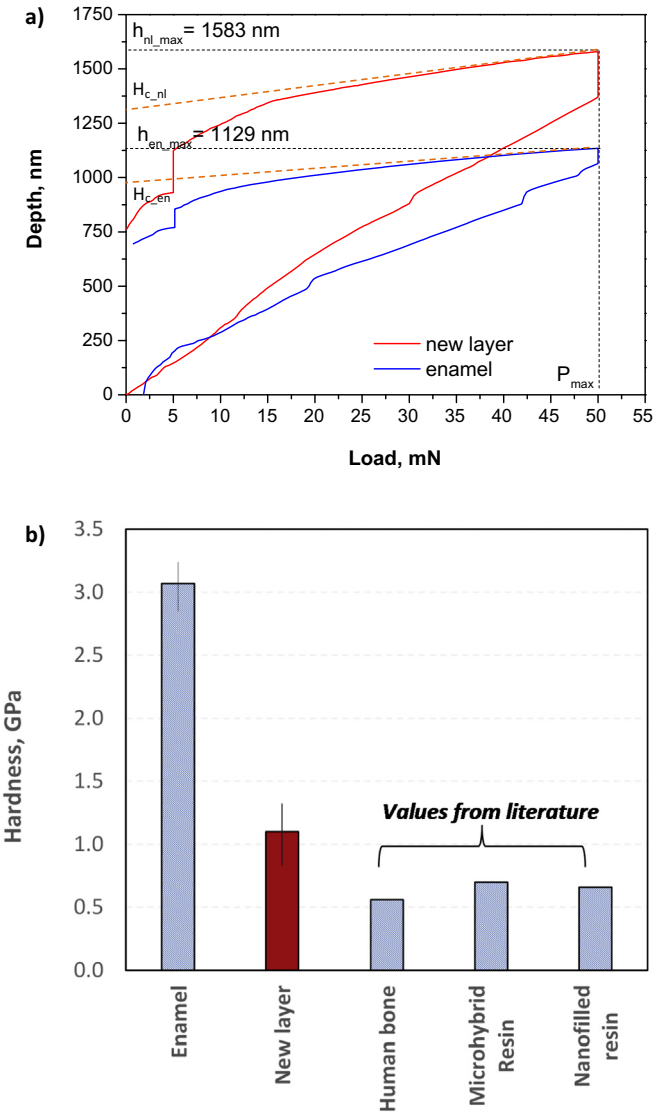

Fig. 6. a) typical hysteresis diagrams for the sintered layer and enamel at a load of 50 mN. Based on the diagram we estimated the indenter displacement at the peak load (h_{max}=1583 nm for the new layer and 1129 nm for enamel), the final depth of the contact impression after unloading (h_f = 754 nm for the new layer and 684 nm for enamel) and the plastic depth for the new layer (H_{c_nl} = 1336 nm); b) hardness of the new layer on enamel (error bar 15%) and comparison with the hardness of dental enamel (error bar 5%), current restorative materials (value from [19]) and human femur bone (value from [20]).

Table 1
Mechanical properties of natural enamel and the sintered layer as measured by nanoindentation. Comparison with current restorative materials and other human hard tissues (typical values from literature).

Material	Hardness, GPa	Young's modulus, GPa	Poisson's ratio
Enamel	3.10 ± 0.12	38.67 ± 1.9	0.25 [23]
Sintered layer	1.10 ± 0.16	20.50 ± 1.2	0.27 [24]
Composite resin	0.50–0.70 [20]	14.4–16.8 [25]	0.26–0.30 [25]
Human bone	0.58–0.80 [21]	17.0–20.0 [21]	

treatment via hyperthermia [26]. Heat is produced upon laser irradiation when the irradiated ions are excited to higher energy states and then relax rapidly via electron-phonon coupling and lattice vibrations. This occurs in transition metal doped materials in the sub-nano second regime [8]. For heat to diffuse from the NPs to the bulk and surrounding material several picoseconds are needed.

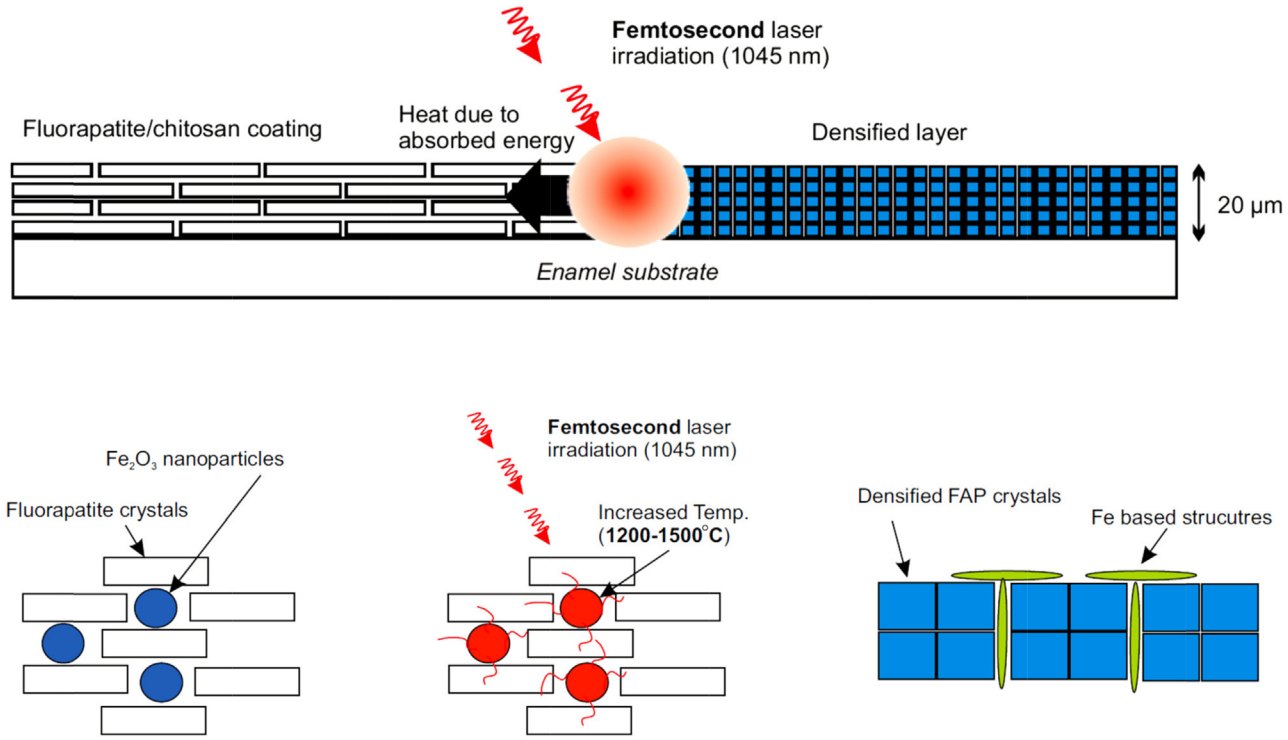

Fig. 7. Illustration of the sintering process during irradiation by an ultrafast, pulsed NIR laser. The iron oxide NPs are distributed in the coating and act as photon absorption centers during laser irradiation. Heat is then transferred to the surrounding FAP crystals resulting in sintering and densification.

Thus, a single femtosecond pulse is a spontaneous heating source with no effect on the bulk material since its duration is 2–4 orders of magnitude shorter than the timescale of heat diffusion. When a high repetition laser is used however, consecutive pulses trigger a cumulative phenomenon resulting in a temperature rise which can potentially reach the melting point of the light absorbing material (in the case of Fe_2O_3 the melting point is 1500 °C). Taking all these into account we can safely assume that in our system iron oxide NPs act as heat generation centers and significantly contribute to the localised heating of the coating and not of the underlying enamel (Fig. 7). During irradiation (0.6 s), heat is transferred from the iron oxide NPs to the surrounding FAP crystals resulting in sintering and densification of these materials (e.g. Fig. 4). Although in this work we utilized a high repetition femtosecond laser to minimize thermal damage on the natural tissue, other systems shouldn't be excluded (e.g. lower repetition rates, longer pulse durations). Heat generation with iron oxide NPs has been reported even with the use of continuous wave lasers [27] but is disputable whether with these systems we can minimize thermal effects on the underlying hard tissues.

Generally, laser assisted sintering of ceramics is a complex process and the exact mechanisms of crystal growth and densification are difficult to characterise. During laser irradiation the temperature distribution is not homogeneous, heating and cooling rates can be rapid (e.g. 2500 °C/s) and the whole process is unlike sintering by conventional heating (e.g. furnaces). From our observations we believe that the maximum temperature in our system would be at the surface of the iron oxide NPs, and we assume that this is close to the melting temperature of this material (i.e. 1500 °C). SEM images of the post sintered surfaces suggest that the iron oxide phase undergoes melting and redistribution before solidification (based on the lamella structures visible in Fig. 3f and g) however, we cannot claim the same for the calcium phosphate crystals. The existence of a liquid phase during laser irradiation implies that the final densified layer is obtained either through a transient liquid phase (if only the iron oxide is liquid) or through a liquid phase sintering mechanism (if both the iron oxide and the ceramic crystals are liquid). We suggest that liquid that is formed under laser irradiation flows between the capillary channels between the FAP particles, fills the pores and causes fusion of the solid particles in contact with the melt (evidenced by the dense microsctructure visible by SEM of cross-sections, Fig. 4). Simultaneous to pore filling, grain growth will take place causing size and morphological changes to the original crystals. In our system phase transformations have been also identified. Post sintering XRD patterns reveal that FAP is transformed to TCP, something which can be only observed for temperatures between 1000 and 1400 °C.

This work introduces a novel methodology for the exogenous re-mineralization of bovine enamel using pulsed lasers and fluorapatite/iron oxide NPs coatings which on optimization should be applicable to human enamel and other hard tissues. Mechanical matching to the underlying enamel with improved wear resistance is achieved through a process that could be transferred to the clinic. It is now possible to clean, paste-coat and then laser irradiate the appropriate powder coating onto a damaged tooth to produce a dense, re-mineralised surface that should have more longevity then existing DH treatments. Further work to realize the translation to the clinic is underway.

5. Conclusions

We have demonstrated that calcium phosphate mineral (FAP) can be sintered and attached to dental enamel without inducing any significant thermal damage to the underlying tissue. This requires, engineering a biomaterial to contain a distribution of iron oxide nanoparticles that may act as heat generation centers during laser irradiation, to drive the localized heating on the coating and not the enamel. Densification and sintering of the coating is

enhanced by the melting of the nanoparticles since mass transport and FAP crystal growth rates are higher in the liquid phase than in the solid. The new layer is proven to be dense and compact to the extent that simulated brushing trials of 15-day duration show little or no mass loss compared to natural enamel. Nano-indentation shows the hardness of the new layer to be lower than that of enamel but significantly higher comparing to current restorative materials and other human hard tissues.

This work successfully demonstrates the concept of direct laser sintering of calcium phosphates on dental hard tissues. More research is needed to optimize the sintered layer's properties (e.g. hardness, stiffness, reduction of micro-cracking and aesthetics) and develop appropriate tools and protocols to allow translation of this methodology into clinic. Although our motivation for this research is the significant clinical need of more permanent restoration of dental enamel, similar approaches may be adapted for other tissue engineering applications.

Acknowledgments

The authors acknowledge support from the sponsors of this work; Marie Curie IF (PRe-FActo), IKC PoF (PRUF), EPSRC LUMIN (EP/K020234/1) and EU-Marie-Curie-IAPP LUSTRE (324538) projects. Also authors would like to acknowledge Mr. Mohammed Javed for the laboratory support and Mr. John Harrington and Mr. Stuart Micklethwaite for SEM support.

Raw data repository: https://doi.org/10.5518/333.

References

[1] A.L. Boskey, Mineralization of bones and teeth, Elements 3 (6) (2007) 385–391.
[2] C. Cao, M. Mei, Q.-L. Li, E. Lo, C. Chu, Methods for biomimetic mineralisation of human enamel: a systematic review, Materials 8 (6) (2015) 2873.
[3] C.J. Kleverlaan, A.J. Feilzer, Polymerization shrinkage and contraction stress of dental resin composites, Dent. Mater. 21 (12) (2005) 1150–1157.
[4] J.F. McCabe, A.W.G. Walls, Applied Dental Materials, Wiley, 2013.
[5] J. Kirkham, A. Firth, D. Vernals, N. Boden, C. Robinson, R.C. Shore, S.J. Brookes, A. Aggeli, Self-assembling peptide scaffolds promote enamel remineralization, J. Dent. Res. 86 (5) (2007) 426–430.
[6] P.A. Brunton, R.P.W. Davies, J.L. Burke, A. Smith, A. Aggeli, S.J. Brookes, J. Kirkham, Treatment of early caries lesions using biomimetic self-assembling peptides - a clinical safety trial, Br. Dent. J. 215 (4) (2013). E6 E6.
[7] L. Chen, K. Liang, J. Li, D. Wu, X. Zhou, J. Li, Regeneration of biomimetic hydroxyapatite on etched human enamel by anionic PAMAM template in vitro, Arch. Oral Biol. 58 (8) (2013) 975–980.
[8] D.Y. Tzou, K.S. Chiu, Temperature-dependent thermal lagging in ultrafast laser heating, Int. J. Heat Mass Transfer 44 (9) (2001) 1725–1734.
[9] A.D. Anastasiou, C.L. Thomson, S.A. Hussain, T.J. Edwards, S. Strafford, M. Malinowski, R. Mathieson, C.T.A. Brown, A.P. Brown, M.S. Duggal, A. Jha, Sintering of calcium phosphates with a femtosecond pulsed laser for hard tissue engineering, Mater. Des. 101 (2016) 346–354.
[10] M.H. Niemz, Laser-Tissue Interactions: Fundamentals and Applications, Springer, 2007.
[11] P. Fischer, M. Locher, V. Romano, H.P. Weber, S. Kolossov, R. Glardon, Temperature measurements during selective laser sintering of titanium powder, Int. J. Mach. Tools Manuf. 44 (12–13) (2004) 1293–1296.
[12] A. Lussi, E. Hellwig, J. Klimek, Fluorides - mode of action and recommendations for use, Schweizer Monatsschrift fur Zahnmedizin = Revue mensuelle suisse d'odonto-stomatologie = Rivista mensile svizzera di odontologia e stomatologia 122 (11) (2012) 1030–1042.
[13] S.Y. Sayenko, Obtaining of strontium doped fluorapatite powders, Funct. Mater. 22 (2) (2015) 263–268.
[14] A.K. Gupta, M. Gupta, Synthesis and surface engineering of iron oxide nanoparticles for biomedical applications, Biomaterials 26 (18) (2005) 3995–4021.
[15] F. Ben Ayed, J. Bouaziz, K. Bouzouita, Pressureless sintering of fluorapatite under oxygen atmosphere, J. Eur. Ceram. Soc. 20 (8) (2000) 1069–1076.
[16] S.-F. Ou, S.-Y. Chiou, K.-L. Ou, Phase transformation on hydroxyapatite decomposition, Ceramics International 39 (4) (2013) 3809–3816.
[17] D.W. Holcomb, R.A. Young, Thermal decomposition of human tooth enamel, Calcified Tissue Int. 31 (1) (1980) 189.
[18] A.D. Anastasiou, S. Strafford, O. Posada-Estefan, C.L. Thomson, S.A. Hussain, T.J. Edwards, M. Malinowski, N. Hondow, N.K. Metzger, C.T.A. Brown, M.N. Routledge, A.P. Brown, M.S. Duggal, A. Jha, β-pyrophosphate: A potential biomaterial for dental applications, Mater. Sci. Eng.: C 75 (2017) 885–894.
[19] A. Lussi, T.S. Carvalho, Erosive tooth wear: a multifactorial condition of growing concern and increasing knowledge, in: A. Lussi, C. Ganss (Eds.), Erosive Tooth Wear From Diagnosis to Therapy, 2014. Monogr Oral Sci. Basel, Karger.
[20] M.R. Galvão, S.G.F.R. Caldas, V.S. Bagnato, A.N. de Souza Rastelli, M.F. de Andrade, Evaluation of degree of conversion and hardness of dental composites photo-activated with different light guide tips, Eur. J. Dentistry 7 (1) (2013) 86–93.
[21] P.K. Zysset, X. Edward Guo, C. Edward Hoffler, K.E. Moore, S.A. Goldstein, Elastic modulus and hardness of cortical and trabecular bone lamellae measured by nanoindentation in the human femur, J. Biomech. 32 (10) (1999) 1005–1012.
[22] W.C. Oliver, G.M. Pharr, An improved technique for determining hardness and elastic modulus using load and displacement sensing indentation experiments, J. Mater. Res. 7 (6) (1992) 1564–1583.
[23] A. Braly, L.A. Darnell, A.B. Mann, M.F. Teaford, T.P. Weihs, The effect of prism orientation in the indentation testing of human molar enamel, Arch. Oral Biol. 52 (9) (2007) 856–860.
[24] O. Prokopiev, I. Sevostianov, Dependence of the mechanical properties of sintered hydroxyapatite on the sintering temperature, Mater. Sci. Eng.: A 431 (1) (2006) 218–227.
[25] J.-H. Park, N.-S. Choi, Equivalent Young's modulus of composite resin for simulation of stress during dental restoration, Dental Mater. 33 (2) (2017) e79–e85.
[26] Z. Bao, X. Liu, Y. Liu, H. Liu, K. Zhao, Near-infrared light-responsive inorganic nanomaterials for photothermal therapy, Asian J. Pharmaceut. Sci. 11 (3) (2016) 349–364.
[27] A. Espinosa, R. Di Corato, J. Kolosnjaj-Tabi, P. Flaud, T. Pellegrino, C. Wilhelm, Duality of iron oxide nanoparticles in cancer therapy: amplification of heating efficiency by magnetic hyperthermia and photothermal bimodal treatment, ACS Nano 10 (2) (2016) 2436–2446.